Semicylindrical microresonator: Excitation, modal structure, and Q-factor

Article *in* Applied Optics · August 2018

DOI: 10.1364/AO.57.006309

4 authors, including:

Hovhannes Haroyan
Yerevan State University
15 PUBLICATIONS **12** CITATIONS
SEE PROFILE

Henrik Parsamyan
Yerevan State University
3 PUBLICATIONS **0** CITATIONS
SEE PROFILE

Kh. Nerkararyan
Yerevan State University
79 PUBLICATIONS **742** CITATIONS
SEE PROFILE

Research Article Vol. 57, No. 22 / 1 August 2018 / Applied Optics 6309

applied optics

Semicylindrical microresonator: excitation, modal structure, and Q-factor

H. Haroyan, H. Parsamyan, T. Yezekyan, and Kh. Nerkararyan*

Department of Radiophysics, Yerevan State University, A. Manoogian 1, Yerevan 0025, Armenia
**Corresponding author: knerkar@ysu.am*

Received 10 April 2018; revised 26 June 2018; accepted 27 June 2018; posted 27 June 2018 (Doc. ID 327931); published 24 July 2018

A semicylindrical microresonator with relatively simple excitation by a plane wave is studied. The resonator is formed on the base of a dielectric/metal/dielectric structure, where the wave energy penetrates into the resonator through a thin metal layer and is stored in a semicylindrical dielectric with high permittivity. The proposed microresonator combines features of Fabry–Perot and whispering-gallery-mode resonators. Dependence of radiation losses on the radius and materials are estimated by theoretical analysis, while excitation by a plane wave is shown via numerical analysis. A quality Q-factor of the resonator up to 10^4 can be achieved at a radius of the semicylinder of several micrometers.

OCIS codes: (230.0230) Optical devices; (140.4780) Optical resonators; (140.3945) Microcavities; (120.2230) Fabry-Perot; (280.4788) Optical sensing and sensors.

https://doi.org/10.1364/AO.57.006309

1. INTRODUCTION

Efficient and low-loss optical coupling to high-quality (Q) factor whispering-gallery-mode (WGM) microresonators [1] is important for a wide range of applications including frequency [2,3] and soliton mode-locked microcombs [4–8], bio- and nano-particle sensors [9–11], cavity optomechanical oscillators [12], Raman lasers [13], and quantum optical devices [14,15]. Dielectric resonators on various platforms (e.g., silica, silicon nitride, lithium niobate) have been monolithically integrated with on-chip waveguides, achieving a loaded Q-factor as high as 10^8 [16–22]. Usually, to achieve phase-matched and mode-matched evanescent wave efficient coupling, it is necessary to use a host material of a resonator with a relatively low refractive index compared to those of standard waveguide coupling materials. In addition, fiber tapers used as unclad waveguides are quite brittle and applicable only for resonators, the refractive index of which is close to the refractive index of fiber. At the same time, waveguide coupling requires diameters (or the couple region) of the resonators to be tens or hundreds of micrometers to achieve effective phase matching. Thus, excitation of high-refractive-index WGM resonators with diameters of a few micrometers is quite challenging [22–24]. Meanwhile, for biosensing purposes, binding of single virions is observed from discrete changes in the resonance frequency of a WGM excited in a microcavity. It is shown that the magnitude of the discrete wavelength-shifted signal can be sufficiently enhanced by reducing the microsphere size [9,25]. On the other hand, effective control of the light wave as a rule is realized using materials with a large refractive index.

Hence, it is interesting to consider microresonators with a high refractive index of the host material and dimensions close to the exciting wavelength.

In this paper, a simple structure of a microresonator with an easy coupling method with an incident plane wave is proposed. The resonator is based on a dielectric/metal/dielectric structure, where the wave energy is stored in the semicylindrical dielectric with a high refractive index (see Fig. 1). The exciting plane wave normally incidents on a dielectric medium (ε_d) with plane-parallel boundaries and penetrates into the semicylinder (ε_s) through a thin metal layer (ε_m).

The proposed resonator combines properties of a Fabry–Perot resonator, where the input of wave energy is carried through mirrors, and a cylindrical resonator, where whispering-gallery ($WG_{m,\ell}$) modes with azimuthal m and radial ℓ mode numbers are formed.

Here, the possibility of simple input and output of radiation is combined with the possibility of using the unique properties of an evanescent wave on the cylindrical surface of a dielectric. Although the values of the Q-factor of the proposed resonator are less than those of planar microdisk and microring resonators, this is quite sufficient for a wide range of investigations.

The investigation is divided into two parts, focused on two aspects of the functioning of the microcavity. At first, an analytical determination of dependence of the radiated field from the curved cylindrical surface of the WGM resonator on the radius and the ratio of the dielectric permittivities of the semicylinder and surrounding is realized. This defines conditions under which the radiation part of the Q-factor is negligible.

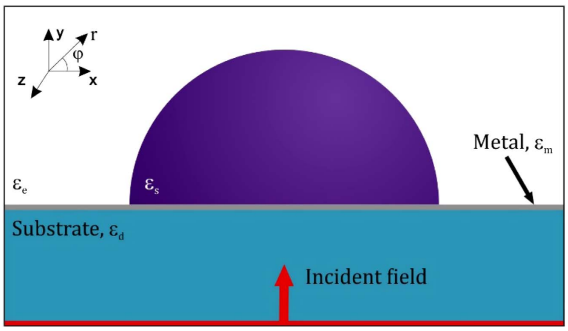

Fig. 1. Cross section of the structure of a semicylindrical microresonator. $\varepsilon_d = 2.25$, $\varepsilon_e = 1$ are dielectric permittivities of the substrate (SiO_2 silica) and the surrounding medium (air), respectively. As a metal and semicylinder medium, Ag and GaAs were used correspondingly.

Second, a numerical study is performed to clarify the possibility of the excitation of a semicylindrical microresonator directly by a plane wave, which determines optimal values of the Q-factor and the role of Joule losses in the metallic layer.

2. THEORY

Let us start with a theoretical study of WGM formation in the proposed structure to identify (determine) the range of values of the radius of a half-cylinder, where the radiation losses of the microcavity can be neglected.

Assume, ε_d, ε_m, ε_s, and ε_e are the permittivities of the substrate, the metal layer, the semicylinder, and the surrounding medium, respectively; R is the radius of the semicylinder; and h is the thickness of the metal layer (see Fig. 1). We use the cylindrical coordinate system (r, φ, z), where z is directed along the axis of the semicylinder. Let us consider the case where the electromagnetic wave, on the side of the dielectric substrate, incidences normally onto the structure (Fig. 1), with the electric field polarized along the axis of the semicylinder (z axis).

The WGMs formed in the semicylindrical resonator are also solutions of the Helmholtz equation in a cylindrical geometry with an additional boundary condition: on the metal surface, the E_z component of the electric field is equal to zero. The Helmholtz equation written in cylindrical coordinates for the axial field of a transverse-magnetic (TM) WGM is:

$$\left(\frac{\partial^2}{\partial r^2} + \frac{1}{r}\frac{\partial}{\partial r} + \frac{1}{r^2}\frac{\partial^2}{\partial \varphi^2} + k_{s,e}^2\right) E_z(r, \varphi, t) = 0, \tag{1}$$

where $k_{s,e} = \sqrt{\varepsilon_{s,e}}\frac{\omega}{c} = \frac{2\pi}{\lambda_{s,e}}$.

Here ω is the angular frequency, $\lambda_{s,e} = \lambda_0/\sqrt{\varepsilon_{s,e}}$ are wavelengths in the semicylinder and surrounding medium, respectively (λ_0 is vacuum wavelength). This equation can be simplified via the method of separation of variables by which it is split into two equations for radial and azimuthal components. These modes consist of azimuthally propagating fields guided by total internal reflection at the dielectric interface and optical interference that prevents the field from penetrating inward beyond a fixed radius.

The appropriate solutions for the radial field dependence both the interior ($r \le R$) and exterior ($r > R$) of the semicylinder are [26]

$$E_z(r, \varphi, t) = AJ_m(k_s r) \cdot \sin(m\varphi) \cdot \exp(i\omega t), \quad \text{at } r \le R, \quad 0 < \varphi < \pi, \tag{2}$$

$$E_z(r, \varphi, t) = BH_m^{(1)}(k_e r) \cdot \sin(m\varphi) \cdot \exp(i\omega t), \quad \text{at } r > R, \quad 0 < \varphi < \pi. \tag{3}$$

Here $J_m(k_s r)$ and $H_m^{(1)}(k_e r)$ are the Bessel and Hankel functions, respectively; m is the azimuthal number ($m = 1, 2, \ldots$); and A and B are unknown constants.

Here we assume that on the surface of the metal layer the tangential component of the electric field is equal to zero. As mentioned before, the aim of this section is to theoretically evaluate radiation losses from the curved cylindrical surface of the resonator; hence, for this purpose, the aforementioned assumption is quite acceptable. However, hereinafter within the numerical analysis to determine conditions for a microcavity excitation by a plane wave, this assumption certainly will not be used.

From the continuity of the tangential components of the field, we can obtain [26,27]

$$\sqrt{\varepsilon_s}\frac{J_m'(k_s R)}{J_m(k_s R)} = \sqrt{\varepsilon_e}\frac{[H_m^{(1)}(k_e R)]'}{H_m^{(1)}(k_e R)}, \tag{4}$$

$$AJ_m(k_s R) = BH_m^{(1)}(k_e R). \tag{5}$$

A family of WGMs naturally come up from the solution of Eq. (4), which are indexed by two mode indices m (azimuthal mode number) and ℓ (the radial mode number) and characterized by resonant frequencies $\omega_{m,\ell}$ [28]. Here, as well as in Eqs. (2) and (3), only explicit dependence on m is present, although the ℓ is defined by the order (m), the argument of the Bessel function, and the radius of the semicylinder. For a fixed wavelength (of an existing mode) and radius, ℓ indicates the number of extremums of the Bessel function of order m to the boundary. It is worth mentioning that from stated boundary conditions (the tangential component of the electric field is equal to zero on the metal surface) it directly follows that the azimuthal mode number is odd (otherwise, surface currents will appear). Note that for a given m, the numbering ℓ is performed with increasing resonant frequency. On the other hand, Eq. (5) gives the relation between the inner and outer fields of the resonator. In further analysis, we are focusing on the WGM of $\ell = 1$ due to the lowest mode volume, which, in fact, is much more valuable from a practical point of view. Particularly, in several experiments with virus-sized polystyrene nanoparticles, it comes out that there is a mechanism for increasing signal by limiting modal volume [25].

The first maximum of the $J_m(k_s r)$ function is when $\ell = 1$ ($WG_{m,1}$) and $m \gg 1$ is located at $k_s r \approx m$. Hence, in the discussed case, $\varepsilon_s \gg \varepsilon_e$ when $k_e R \ll m$; for estimations we can use following approximations [29]:

$$H_m^{(1)}(k_e R) \approx -i\frac{(m-1)!}{\pi}\left(\frac{2}{k_e R}\right)^m, \tag{6}$$

$$J_m(m) \approx \frac{2^{1/3}}{3^{2/3}\Gamma(2/3)}\frac{1}{m^{1/3}}, \tag{7}$$

$$m! \approx m^m \exp(-m)\sqrt{2\pi m}. \tag{8}$$

Finally, the relation between constants of inner and outer fields has following form:

$$B \approx iA\sqrt{\frac{\pi m^{1/3}}{2^{1/3}}}\frac{1}{3^{2/3}\Gamma(2/3)}\left(\frac{e}{2}\sqrt{\frac{\varepsilon_e}{\varepsilon_s}}\right)^m, \tag{9}$$

where $m \approx 2\pi R/\lambda_s$.

Note that the dependence of the $|B|/|A|$ on the semicylinder radius R [which is derived from Eq. (9) and the relation between m and R] is an exponentially decaying function. Since the radiative part of the Q-factor of the resonator is proportional to the ratio $|A|^2/|B|^2$, therefore from Eq. (9) it is possible to determine conditions when radiation from the curved boundary is negligible (which is possibly realized), and the Q-factor of the resonator is mainly determined by the radiation from the metal layer and the Joule losses.

3. NUMERICAL ANALYSIS AND DISCUSSION

Now, let us consider the problem of the excitation of WGM in a semicylindrical microresonator by a plane wave. Numerical analysis based on finite element method is carried out for the following values of the parameters $\varepsilon_d = 2.25$, $\varepsilon_e = 1$, $R = 3$ μm, and $h = 80$ nm; the values of ε_m (as a metal we use silver) and ε_s (as a semiconductor we use GaAs) have been chosen according to Ref. [30] and [31], respectively.

The characteristic images for the electric field distributions (E_z component) of modes with a relatively high Q are presented in Fig. 2. The Q-factor of the resonator was determined by the equation $Q \approx \lambda_p/\Delta\lambda$, where λ_p and $\Delta\lambda$ are the peak wavelength and the full width at half-maximum, respectively. $\Delta\lambda$ was determined from the curve of dependence of the square of the amplitude of the field on the wavelength. In the investigated case, like in the case of traditional WGM resonators, the Q-factor of the resonator is proportional to the radius; the bigger radius, the higher the Q-factor. It should be noted that the calculations carried out according to Eq. (2) and the results obtained by numerical calculations perfectly correspond to each other.

To optimize metal thickness, it is interesting to investigate the dependencies of the electric field inside the resonator and the Q-factor on metal thickness h. To carry out the dependence of the square of electric field amplitude ($|A|^2$) on the metal thickness, we fixed the resonant wavelength at 1012.98 nm and changed the metal thickness in range of 50–120 nm. After that, we derived the maximum value of the $|A|^2$ within the semicylinder. Second, to derive the dependence of the Q-factor of $WG_{59,1}$ on the metal thickness, we changed the metal thickness and determined the Q-factor by the same way as for Fig. 2. Numerical calculations show that Q-factor increases by increasing the thickness of the metal layer and saturates approximately starting from $h = 80$ nm (see Fig. 3). Meanwhile, the square of the amplitude of the z component of the electric field (or, in essence, the wave energy stored in the microcavity) reaches a maximum at $h = 65$ nm, after which it decreases monotonically. Such a seeming discrepancy can be explained only by a rather rapid decrease in the total (radiation and Joule) losses of the microcavity.

The point is that by increasing the thickness of the metal layer, the value of the electric component of the standing wave on the surface of the metal layer promptly tends to zero.

In this context it is important to indicate the dielectric constants of Ag (ε_m) and GaAs (ε_s) at resonant wavelengths $\varepsilon_m = -52.068 + 0.57727i$ and $\varepsilon_s = 12.2444$ at $\lambda_0 = 1012.98$ nm ($WG_{59,1}$), $\varepsilon_m = -55.7 + 0.59707i$ and $\varepsilon_s = 12.132$ at $\lambda_0 = 1045.05$ nm ($WG_{33,7}$), $\varepsilon_m = -56.481 + 0.60124i$ and $\varepsilon_s = 12.1097$ at $\lambda_0 = 1051.8$ nm ($WG_{39,5}$).

Thus, in order to maximize the wave fields in the microcavity, it is necessary to choose a certain thickness of the metal layer, while for maximizing the Q-factor, another value should be chosen. Hence, an optimal thickness of the metal layer must be picked to satisfy the demands of relatively high values of wave field amplitude in the microcavity and at the same time preserving reasonable values of the Q-factor. Note that $h = 80$ nm ensures both high values of the Q-factor and relatively high values of the field inside the resonator. This creates favorable conditions for the registration of the process and has an important role in terms of the vastness of the applications.

For parameters used in the numerical analysis, the $|B|/|A|$ derived from Eq. (9) is approximately 10^{-8}, and hence the radiative losses from the curved boundary are negligible. A relatively

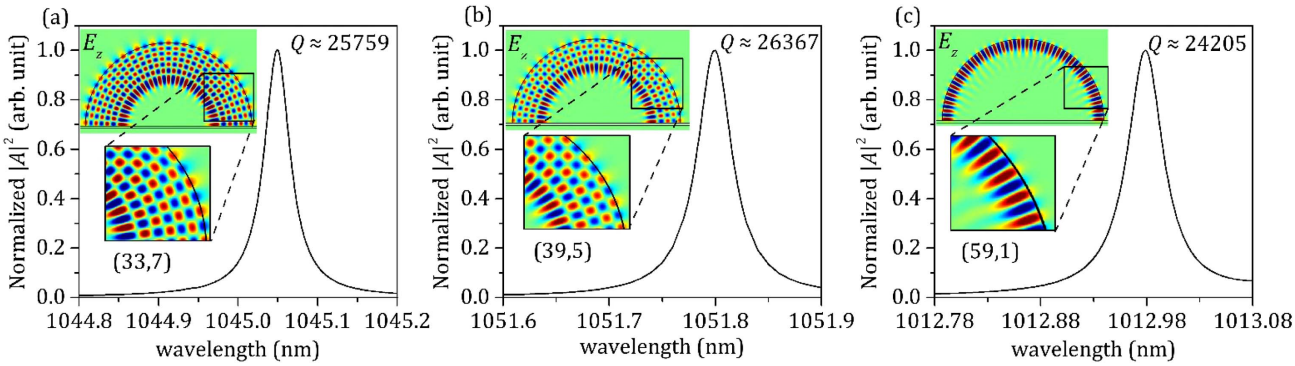

Fig. 2. Distributions of the electric filed E_z component amplitudes of particular modes, resonance curves, and Q-factors: (a) $m = 33$, $\ell = 7$ ($WG_{33,7}$), $\lambda_0 = 1045.05$ nm; (b) $m = 39$, $\ell = 5$ ($WG_{39,5}$), $\lambda_0 = 1051.8$ nm; and (c) $m = 59$, $\ell = 1$ ($WG_{59,1}$), $\lambda_0 = 1012.98$ nm. The model parameters are: $\varepsilon_d = 2.25$, $\varepsilon_e = 1$, $R = 3$ μm, $h = 80$ nm. As the metal and material of the semicylinder, silver (Ag) and GaAs were used, correspondingly.

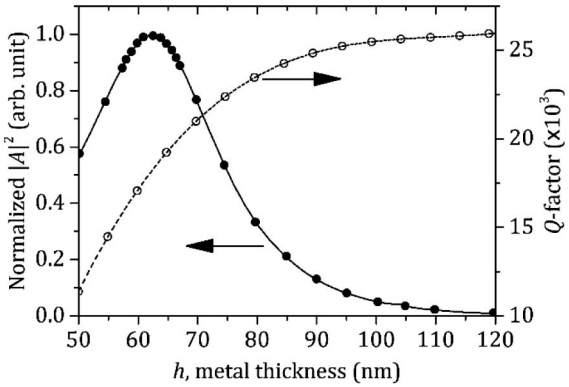

Fig. 3. Dependences of the normalized square of electric field amplitude $|A|^2$ (left axis) and Q-factor (right axis) on the thickness h of the metal layer for the $WG_{59,1}$ mode.

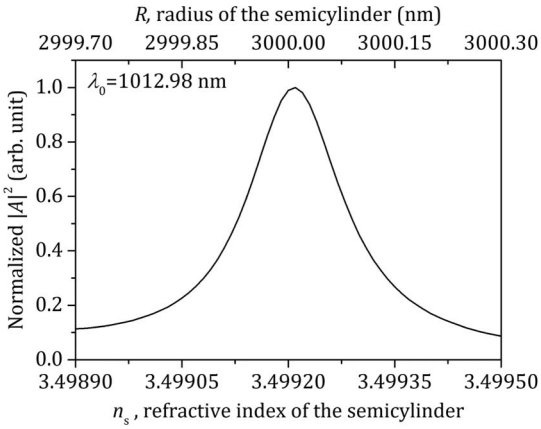

Fig. 4. Dependence of the square of the electric field amplitude $|A|^2$ on the refractive index of the medium filled in half-cylinder n_s (bottom axis) and on the radius of half-cylinder R (top axis) for the $WG_{59,1}$ resonant mode. The metal thickness $h = 80$ nm for the surrounding medium $\varepsilon_e = 1$. Note that top and bottom axes are independent.

high value of the Q-factor ensures the extreme sensitivity of the wave energy stored in the resonator from the number of parameters. In particular, a noticeable change of the wave energy stored in the resonator with a change in the refractive index $n_s = \sqrt{\varepsilon_s}$ of the semicylinder by $\Delta n_s \approx 10^{-4}$ opens up wide possibilities for light control by using various nonlinear and electro-optical effects (see Fig. 4, bottom axis). It is noteworthy that the wave energy is weakly dependent on the refractive index of the surrounding medium.

Another interesting feature is that the energy stored in the resonator significantly depends on the semicylinder's radius (see Fig. 4, top axis).

From numerical calculations it follows that in the resonant regime stored energy significantly changes by varying the radius of the semicylinder, even when changing by the decimal part of a nanometer. This circumstance gives a basis to conclude that the investigated system is able to register the presence of a molecular thin layer absorbed by the semicylindrical resonator.

4. CONCLUSION

Thus, based on the dielectric/metal/insulator structure, an optical microresonator can be designed where the wave energy is stored in a semicylindrical dielectric with a relatively high permittivity. Here, the exciting wave falls from the side of another dielectric and penetrates into the microcavity through a thin metal layer, thereby creating favorable conditions for an easily coupling. The proposed microresonator combines the properties of a Fabry–Perot resonator, where the input of the wave energy is carried out through a mirror (metal layer), and a cylindrical resonator, where WGMs are formed.

Dependence of radiation losses on the radius and materials are estimated by theoretical analysis, while excitation by a plane wave is shown via numerical analysis.

Calculations show that the Q-factor up to 10^4 can be achieved, which is competitive with other WGM resonators with sizes of several micrometers. The high values of Q ensure the extreme sensitivity of the wave energy stored in the resonator from the number of parameters. In particular, a noticeable change of the wave energy stored in the resonator by the alteration of the refractive index of the semicylinder by $\Delta n_s \approx 10^{-4}$ opens up wide possibilities for light control using various nonlinear and electro-optical effects. The energy stored in the resonator significantly depends on the semicylinder radius, which makes it possible to use as a sensor for detection of the absorbed molecular thin layers. The simple way to experimentally study the process of accumulating wave energy is to measure the output power from the cylindrical surface by evanescent coupling. In the case of the formation of a resonance mode, the output power should drastically increase. Another way is the measurement of the reflected field disruption from the metal layer.

Funding. Ministry of Education and Science of Armenia, Science Committee (15T-1C146, GE-027).

REFERENCES

1. K. J. Vahala, "Optical microcavities," Nature **424**, 839–846 (2003).
2. P. Del'Haye, A. Schliesser, O. Arcizet, T. Wilken, R. Holzwarth, and T. J. Kippenberg, "Optical frequency comb generation from a monolithic microresonator," Nature **450**, 1214–1217 (2007).
3. T. J. Kippenberg, R. Holzwarth, and S. A. Diddams, "Microresonator-based optical frequency combs," Science **332**, 555–559 (2011).
4. T. Herr, V. Brasch, J. D. Jost, C. Y. Wang, N. M. Kondratiev, M. L. Gorodetsky, and T. J. Kippenberg, "Temporal solitons in optical microresonators," Nat. Photonics **8**, 145–152 (2014).
5. X. Yi, Q.-F. Yang, K. Y. Yang, M.-G. Suh, and K. Vahala, "Soliton frequency comb at microwave rates in a high-Q silica microresonator," Optica **2**, 1078–1085 (2015).
6. V. Brasch, M. Geiselmann, T. Herr, G. Lihachev, M. H. P. Pfeiffer, M. L. Gorodetsky, and T. J. Kippenberg, "Photonic chip-based optical frequency comb using soliton Cherenkov radiation," Science **351**, 357–360 (2016).
7. C. Joshi, J. K. Jang, K. Luke, X. Ji, S. A. Miller, A. Klenner, Y. Okawachi, M. Lipson, and A. L. Gaeta, "Thermally controlled comb generation and soliton modelocking in microresonators," Opt. Lett. **41**, 2565–2568 (2016).
8. P.-H. Wang, J. A. Jaramillo-Villegas, Y. Xuan, X. Xue, C. Bao, D. E. Leaird, M. Qi, and A. M. Weiner, "Intracavity characterization of microcomb generation in the single-soliton regime," Opt. Express **24**, 10890–10897 (2016).

9. F. Vollmer and S. Arnold, "Whispering-gallery-mode biosensing: label-free detection down to single molecules," Nat. Methods **5**, 591–596 (2008).
10. T. Lu, H. Lee, T. Chen, S. Herchak, J.-H. Kim, S. E. Fraser, R. C. Flagan, and K. Vahala, "High sensitivity nanoparticle detection using optical microcavities," Proc. Natl. Acad. Sci. USA **108**, 5976–5979 (2011).
11. F. Vollmer and L. Yang, "Label-free detection with high-Q microcavities: a review of biosensing mechanisms for integrated devices," Nanophotonics **1**, 267–291 (2012).
12. T. J. Kippenberg and K. J. Vahala, "Cavity optomechanics: back-action at the mesoscale," Science **321**, 1172–1176 (2008).
13. S. M. Spillane, T. J. Kippenberg, and K. J. Vahala, "Ultralow-threshold Raman laser using a spherical dielectric microcavity," Nature **415**, 621–623 (2002).
14. T. Aoki, B. Dayan, E. Wilcut, W. P. Bowen, A. S. Parkins, T. J. Kippenberg, K. J. Vahala, and H. J. Kimble, "Observation of strong coupling between one atom and a monolithic microresonator," Nature **443**, 671–674 (2006).
15. H. J. Kimble, "The quantum internet," Nature **453**, 1023–1030 (2008).
16. L. Razzari, D. Duchesne, M. Ferrera, R. Morandotti, S. Chu, B. E. Little, and D. J. Moss, "CMOS-compatible integrated optical hyper-parametric oscillator," Nat. Photonics **4**, 41–45 (2010).
17. J. S. Levy, A. Gondarenko, M. A. Foster, A. C. Turner-Foster, A. L. Gaeta, and M. Lipson, "CMOS-compatible multiple-wavelength oscillator for on-chip optical interconnects," Nat. Photonics **4**, 37–40 (2010).
18. D. T. Spencer, J. F. Bauters, M. J. R. Heck, and J. E. Bowers, "Integrated waveguide coupled Si^3N^4 resonators in the ultrahigh-Q regime," Optica **1**, 153–157 (2014).
19. M. Zhang, C. Wang, R. Cheng, A. Shams-Ansari, and M. Lončar, "Monolithic ultra-high-Q lithium niobate microring resonator," Optica **4**, 1536–1537 (2017).
20. P. Del'Haye, T. Herr, E. Gavartin, M. L. Gorodetsky, R. Holzwarth, and T. J. Kippenberg, "Octave spanning tunable frequency comb from a microresonator," Phys. Rev. Lett. **107**, 063901 (2011).
21. A. Gondarenko, J. S. Levy, and M. Lipson, "High confinement micron-scale silicon nitride high Q ring resonator," Opt. Express **17**, 11366–11370 (2009).
22. K. Y. Yang, D. Y. Oh, S. H. Lee, Q.-F. Yang, X. Yi, B. Shen, H. Wang, and K. Vahala, "Bridging ultrahigh-Q devices and photonic circuits," Nat. Photonics **12**, 297–302 (2018).
23. G. Liu, V. S. Ilchenko, T. Su, Y.-C. Ling, S. Feng, K. Shang, Y. Zhang, W. Liang, A. A. Savchenkov, A. B. Matsko, L. Maleki, and S. J. Ben Yoo, "Low-loss prism-waveguide optical coupling for ultrahigh-Q low-index monolithic resonators," Optica **5**, 219–226 (2018).
24. A. B. Matsko and V. S. Ilchenko, "Optical resonators with whispering-gallery modes-part I: basics," IEEE J. Sel. Top. Quantum Electron. **12**, 3–14 (2006).
25. F. Vollmer, S. Arnold, and D. Keng, "Single virus detection from the reactive shift of a whispering-gallery mode," Proc. Natl. Acad. Sci. USA **105**, 20701–20704 (2008).
26. A. Chiasera, Y. Dumeige, P. Féron, M. Ferrari, Y. Jestin, G. Nunzi Conti, S. Pelli, S. Soria, and G. C. Righini, "Spherical whispering-gallery-mode microresonators," Laser Photon. Rev. **4**, 457–482 (2010).
27. M. A. Kaliteevski, S. Brand, R. A. Abram, A. Kavokin, and L. S. Dang, "Whispering gallery polaritons in cylindrical cavities," Phys. Rev. B **75**, 233309 (2007).
28. M. R. Foreman, J. D. Swaim, and F. Vollmer, "Whispering gallery mode sensors," Adv. Opt. Photon. **7**, 168–240 (2015).
29. M. Abramowitz and I. A. Stegun, *Handbook of Mathematical Functions* (Dover, 1965).
30. P. B. Johnson and R. W. Christy, "Optical constants of the noble metals," Phys. Rev. B **6**, 4370–4379 (1972).
31. T. Skauli, P. S. Kuo, K. L. Vodopyanov, T. J. Pinguet, O. Levi, L. A. Eyres, J. S. Harris, M. M. Fejer, B. Gerard, L. Becouarn, and E. Lallier, "Improved dispersion relations for GaAs and applications to nonlinear optics," J. Appl. Phys. **94**, 6447–6455 (2003).